https://doi.org/10.5194/acp-2020-109
Preprint. Discussion started: 16 March 2020
© Author(s) 2020. CC BY 4.0 License.

Atmospheric Chemistry and Physics Discussions

Variations in N_{cn} and N_{ccn} over China marginal seas related to marine traffic emissions, new particle formation and aerosol aging

Yang Gao[1,2#*], Deqiang Zhang[1#], Juntao Wang[1], Huiwang Gao[1, 2] and Xiaohong Yao[1, 2*]

[1]Frontiers Science Center for Deep Ocean Multispheres and Earth System, and Key Laboratory of Marine Environment and Ecology, Ministry of Education, Ocean University of China, Qingdao, 266100, China

[2]Laboratory for Marine Ecology and Environmental Science, Qingdao National Laboratory for Marine Science and Technology, Qingdao, 266237, China

[#]Authors contribute equally to this study

[*]Correspondence to yanggao@ouc.edu.cn; xhyao@ouc.edu.cn

https://doi.org/10.5194/acp-2020-109
Preprint. Discussion started: 16 March 2020
© Author(s) 2020. CC BY 4.0 License.

Atmospheric Chemistry and Physics Discussions

Abstract

In this study, a cruise campaign was conducted over China marginal seas to measure concentrations of condensation nuclei (N_{cn}), cloud condensation nuclei (N_{ccn}) and other pollutants during DOY 110 to DOY 135 of 2018. With exhaustedly excluded self-ship emission signals, the mean values of N_{ccn} during the cruise campaign slightly increased from $3.2 \pm 1.1 \times 10^3$ cm^{-3} (mean ± standard) at supersaturation (SS) of 0.2% to $3.9 \pm 1.4 \times 10^3$ cm^{-3} at SS of 1.0%, and the mean value for N_{cn} was $8.1 \pm 4.4 \times 10^3$ cm^{-3}. Data analysis showed that marine traffic emissions apparently yielded a large contribution to the increase of N_{cn} in daytime, especially in marine atmospheres over their heavily travelled sea zones; however, the fresh sources had no clear contribution to the increase of N_{ccn}. This finding was supported by the quantitative relations between N_{cn} and N_{ccn} at SS=0.2-1.0% against mixing ratios of SO_2 in self-ship emission plumes, i.e., 1 ppb increase in SO_2 corresponds to 1.4×10^4 cm^{-3} increase in N_{cn}, but only 30-170 cm^{-3} increase in N_{ccn} possibly because of abundant organics in the aerosols. The smooth growth of marine traffic derived particles can be observed, reflecting aerosol aging. The estimated hygroscopicity parameter (κ) values were generally as high as 0.46-0.55 under the dominant onshore winds, suggesting inorganic ammonium aerosols likely acting as the major contributor to N_{ccn} through aerosol aging processes largely decomposed organics. Moreover, the influences of the transported new particles from the continent on N_{cn} and N_{ccn} in the marine atmosphere were also investigated.

Key words: N_{cn}; N_{ccn}; marine traffic emissions; hygroscopicity parameter; SO_2

https://doi.org/10.5194/acp-2020-109
Preprint. Discussion started: 16 March 2020
© Author(s) 2020. CC BY 4.0 License.

1. Introduction

Oceans occupy approximately 2/3 of the Earth's surface and water evaporation from oceans acts as the major source of moisture in the atmosphere. Aerosol-cloud interactions in marine atmospheres, covering from tropics to polar regions, thereby attract great attentions in the past few decades due to their impact on the climate change (Brooks and Thornton, 2018; Huebert et al., 2003; Quinn and Bates, 2011; Rosenfeld et al., 2019; Wang et al., 2014; Yu and Luo, 2009). However, large uncertainties still exist in various marine atmospheres, e.g., the sources of aerosols, concentrations of bulk cloud condensation nuclei (CCN) and aerosol CCN activation under various of supersaturation, etc. (Clarke et al., 2006; Decesari et al., 2011; Quinn and Bates, 2011; Rosenfeld et al., 2019; Saliba et al., 2019). The uncertainties are mainly determined by limited observations in marine atmospheres, although a few additional observations of number concentrations of aerosol (N_{cn}) and CCN (N_{ccn}) were recently reported in different marine atmospheres, e.g., over Mediterranean, Sea of Japan, Bay of Bengal, coast of California and the Northwest Pacific Ocean etc. (Bougiatioti et al., 2009; Ramana and Devi, 2016; Ruehl et al., 2009; Wang et al., 2019; Yamashita et al., 2011).

Including sea-spray aerosols and secondarily formed aerosols from sea-derived gaseous precursors (Blot et al., 2013; Clarke et al., 2006; Fossum et al., 2018; O'Dowd et al., 1997; Quinn and Bates, 2011), marine traffics also emit a large amount of aerosols and reactive gases (Chen et al., 2017a). These pollutants may also directly or indirectly contribute to CCN therein, to some extent (Langley et al., 2010). In addition, the long-range transport of continental aerosols widely reportedly acted as an important source of CCN in marine atmospheres (Charlson et al., 1987; Fu et al., 2017; Huebert et al., 2003; Royalty et al., 2017; Sato and Suzuki, 2019; Wang et al., 2019). The continent-derived aerosol particles observed in marine atmospheres usually mix with different sources such as biomass burning, dust and anthropogenic emissions (Feng et al., 2017; Guo et al., 2014; Guo et al., 2016; Lin et al., 2015). An appreciable fraction of organics

https://doi.org/10.5194/acp-2020-109
Preprint. Discussion started: 16 March 2020
© Author(s) 2020. CC BY 4.0 License.

reportedly exists in marine aerosols and continental aerosols upwind of oceans (Ding et al., 2019; Feng et al., 2012; Feng et al., 2016; O'Dowd et al., 2004; Quinn et al., 2015; Song et al., 2018). However, ammonium sulfate aerosols have been frequently reported to dominantly contribute to CCN-related aerosols in many marine atmospheres and lead to hygroscopicity parameter (κ) larger than 0.5 (Cai et al., 2017; Fu et al., 2017; Mochida et al., 2010; Phillips et al., 2018; Royalty et al., 2017). A question is automatically raised, i.e., where do particulate organics go in the marine aerosols enriched in ammonium sulfate? Anthropogenic emission such as SO_2, NO_x in general increase since 1980s, until recently started to decrease, i.e., SO_2 start to decrease from 2006 (Li et al., 2017) whereas NOx started to decrease since 2011 (Li et al., 2017; Liu et al., 2016). Together with the influence of the Asian Monsson, the marginal seas of China are, therefore, inevitably affected by the outflow of continent al aerosols (Feng et al., 2017; Guo et al., 2016). Observations of N_{cn} and N_{ccn} in marine atmospheres over China marginal seas helps to resolve the data scarcity, understand their sources and dynamic changes and better service the study of their potential climate impacts.

In this study, cruise campaigns were conducted to measure the N_{ccn}, N_{cn}, particle number size distributions, gaseous pollutants and aerosol composition of water-soluble ionic species over the marginal seas from 20 April 2018 (day of year (DOY) 110) to 15 May 2018 (DOY 135), traveling from the East China sea to the South China sea, and returning to the Yellow sea. Spatiotemporal variations in N_{cn}, N_{ccn} and CCN activities of aerosol particles were studied. The *Kappa* values of aerosol particles from DOY 110 to DOY 118 over the marine were calculated and analyzed. Finally, we tried to establish the correlations of N_{cn} and N_{ccn} with mixing ratios of SO_2 in self-ship plumes and ambient marine air. The correlation equations are valuable for a rough estimation of N_{cn} and N_{ccn} from SO_2 when their direct observations are not available.

2. Experimental design

2.1 Instruments and data sources

https://doi.org/10.5194/acp-2020-109
Preprint. Discussion started: 16 March 2020
© Author(s) 2020. CC BY 4.0 License.

A cruise campaign was conducted across China marginal seas, including the East China sea, the South China sea and the Yellow sea from Day of Year (DOY) 110 to DOY 135 of 2018 (Fig. 1a,b). A suite of instruments including a Fast Mobility Particle Sizer (FMPS, TSI Model 3091), CCN counter (CCNC, DMT Model 100), Condensation Particle Counter (CPC, TSI Model 3775), gas analyzers, Ambient Ion Monitor-Ion chromatography (AIM-IC) etc., were onboard a commercial cargo ship *Anqiang 87* for measurements. The FMPS were used to measure particle number size distributions with mobility diameters from 5.6 nm to 560 nm in 32 channels at 1-second temporal resolution with an inlet flow of 10 L min^{-1}. The CPC were used to report the total number concentrations of particles in the range of 3-3000 nm (N_{cn}) in 2-second time resolution with an inlet flow of 1.5 L min^{-1}. The N_{cn} was then used to calibrate the particle number size distributions simultaneously measured by the FMPS, on basis of the procedure proposed by Zimmerman et al. (2015). Due to the severe oceanic condition and humid weather conditions, the FMPS and CPC were out of service after DOY 118 and DOY 122, respectively. Prior to the campaign, the CCNC was calibrated with ammonium sulfate particles based on the standard procedure detailed at Rose et al. (2008). The total flow rate of CCNC was 0.45 L min^{-1}, with a ratio of sample to sheath at 1/10, and five super saturations (SS) conditions were selected including 0.2 %, 0.4 %, 0.6 %, 0.8 %, and 1.0 %. More detailed information about the collection of CCN can be found in Wang et al. (2019).

During the measurement, ambient particles were first sampled through a conductive tube (TSI, US) and a diffusion dryer filled with silica gel (TSI, US), and then splitted into different instruments with a splitter. All instruments were placed in an air-conditioned container on the deck of ship, with inlet height of approximately 6 m above the sea level. Regarding the gas analyzers, the ambient O_3 (Model 49i, Thermo Environmental Instrument Inc., USA C-series), SO_2 (Model 43i, Thermo Environmental Instrument Inc., USA C-series), and NO_x (Model 42i, Thermo Environmental Instrument Inc., USA C-series) were measured in mixing ratios with temporal resolution of one-minute. The CCNC and gas analyzers were operated

https://doi.org/10.5194/acp-2020-109
Preprint. Discussion started: 16 March 2020
© Author(s) 2020. CC BY 4.0 License.

properly throughout the entire campaign. The same was true for Ambient Ion Monitor-Ion chromatography (AIM-IC), which was used to measure water-soluble ionic species in ambient particles less than 2.5 μm.

In this study, the Hybrid Single-Particle Lagrangian Integrated Trajectory (HYSPLIT) model from the NOAA Air Resources Laboratory was used to track the particle sources. The input of HYSPLIT such as wind speed and wind direction was from European Centre for Medium-Range Weather Forecasts (ECMWF). Meanwhile, the data of fire spots was available at the Fire Information for Resource Management System (FIRMS;http://firefly.geog.umd.edu/firemap).

The hygroscopicity parameter (κ) was calculated according to the method proposed by Petters and Kreidenweis (2007).

$$\kappa = \frac{4A^3}{27D_d^3 \ln^2 S_C}, \quad A = \frac{4\sigma_{s/a} M_w}{RT\rho_w}$$

where D_d is the dry diameter, S_C is the super saturation, , M_w is the molecular weight of water, $\sigma_{s/a}$, as a constant of 0.072 J m^{-2}, represent the surface tension over the interface of the solution and air, R is the universal gas constant, T is the ambient temperature and ρ_w is the water density. The FMPS has a low size resolution, particularly at the size greater than 90 nm, which doesn't allow accurately calculating *Kappa* values at SS=0.2%. At SS=0.6% and 0.8%, the *Kappa* value was not calculated considering the complication in the explanation of the value, possibly reflecting the combined effects of particle size, mixing state and chemical composition.

2.2 Separating ambient signals of N_{cn} and N_{ccn} from self-ship emission signals

The data measured during the cruise campaign were frequently interfered by self-ship emission signals. Ambient and self-ship emission signals of N_{cn} and N_{ccn} over the marginal seas were first distinguished from each other and studied separately. The data measured at 18:00-24:00 on DOY 115 were used to illustrate the separation, with the size distribution of particle number concentration during DOY 110-118 shown in Fig.

https://doi.org/10.5194/acp-2020-109
Preprint. Discussion started: 16 March 2020
© Author(s) 2020. CC BY 4.0 License.

S1-S9 in the supporting information. At 18:00-21:11 LT (Local Time), the low N_{cn} of $5.8\pm0.4\times10^3$ cm^{-3} were observed. The accumulation mode dominated in particle number concentration with the median mobility mode diameter at 105±4 nm (Fig. 2a). Afterwards, the N_{cn} rapidly increased by over one order of magnitude (Fig. 2b). The dominant particle number concentration mode changed from accumulation mode to Aitken mode, with the median mobility diameter of Aitken mode stabilized at 47±4 nm in approximately 90% of the time. The rapid increase in N_{cn} and the change in mode size indicated the signal of ship emission itself. The self-ship emission interference after 21:11 was also supported by additional evidences, e.g., a large decrease in activation ratio (AR), defined as the quotient of N_{ccn} and N_{cn}, from >0.5 to <0.2 at SS=0.4% (Fig. 2c) due to large increase of N_{cn} but much smaller magnitude enhancement of N_{ccn} (Fib. 2b), a rapid increase of NO_x from <10 ppb to 192±99 ppb, NO/NO_2 from <0.1 to 0.7±0.3, as well as SO_2 from <2 ppb to 6.2±2.4 ppb. The large changes were expected because the ship smoke stock was approximately only 10 meters away from these detectors. Thus, based upon the feature described above certain criteria were designed in this study to identify self-ship emission signals so as to separate from ambient signals, i.e., a net increase in N_{cn} beyond 5×10^4 cm^{-3} in five minutes, the median mobility mode diameter around 50 nm, NO_2>30 ppb and NO/NO_2>0.5. Please note that there was a short period lasting a few minutes during the transition of signals dominant by either ambient environment or self-ship emission. which was excluded from the following analysis.

3. Results and discussion

3.1 Spatiotemporal variations in ambient N_{cn} during the cruise period

Fig. 3 shows a time series of minutely averaged distributions of N_{cn}, N_{ccn} and AR at SS of 0.4% and 1.0% from DOY 110 to DOY 135 2018, when self-ship emission signals had been exhaustedly removed.

When spatiotemporal variations in N_{cn} were examined during the first half cruise period （Fig. 3a）, the N_{cn} spanned a broad range of $0.2\text{-}4.5\times10^4$ cm^{-3} with the average value

https://doi.org/10.5194/acp-2020-109
Preprint. Discussion started: 16 March 2020
© Author(s) 2020. CC BY 4.0 License.

of 8.1 ± 4.4×10^3 cm^{-3}. Specifically, the N_{cn} were only 6.5 ± 0.8×10^3 cm^{-3} at 00:00-06:00 LT on DOY110 when the ship anchored at the Yangtze River estuary near Shanghai (Fig. 1). The low N_{cn} were comparable to the mean value of N_{cn} (5.4×10^3 cm^{-3}) in marine-air cases during January-December 2010 in Shanghai reported by Leng et al. (2013). The N_{cn} largely increased to 1.9 ± 0.7×10^4 cm^{-3} at 08:00-21:00 LT on DOY110 when the ship cruised across the Yangtze River estuary. The measured particles in number concentration were dominantly distributed at Aitken mode on that day while the median Aitken mode diameter shifted from 49±5 nm at 00:00-06:00 to 40±5 nm at 08:00-21:00 (Fig. S1). The Yangtze River estuary contains several world-class ports and is heavily travelled by marine traffics in daytime (Chen et al., 2017). Since the onshore wind dominated on that day (not shown), the increase in N_{cn} and the decrease in median Aitken mode diameter at 08:00-21:00 LT possibly reflected the increased contribution from marine traffic emissions. Marine traffics visibly decreased when the ship left the Yangtze River estuary toward the south. The N_{cn} were then significantly decreased, i.e., 9.5 ± 4.4×10^3 cm^{-3} in the marine atmosphere over the sea zone in Zhejiang Province (at 07:00 LT on DOY111 - 17:00 LT on DOY 114), with $P<0.01$. The N_{cn} further decreased to the lower values of 5.8 ± 1.7×10^3 cm^{-3} in the marine atmosphere over the sea zone in Fujian Province (at 18:00 LT on DOY114 - 14:00 LT on DOY 117). All these values were, however, 1-2 orders of magnitude larger than the background values in remote clear marine atmospheres, e.g., <300 particle cm^{-3} without the influence of industrial activities in the western Pacific and the tropical Pacific (Ueda et al., 2016) and those reported by Quinn and Bates (2011) and Saliba et al. (2019), indicating overwhelming contributions from non-sea-spray aerosols including marine traffic emissions, the long-range continental transport, newly formed particles in marine atmospheres, etc. As reported, atmsopheric particles over China marginal seas can be further transported to the remote northwest Pacific Ocean (NWPO) in spring under westerly winds, e.g., N_{cn} observed over the NWPO in March-April 2014 were as high as 2.8±1.0 ×10^3 cm^{-3} and approxiately half of that over China marginal seas observed in March 2014 (Wang et al., 2019).

The mean value of N_{cn} (8.1 ± 4.4×10^3) observed in this study was close to that of 7.6 ± 4.0×10^3 cm^{-3} (the number concentrations of particles larger than 10 nm) over the eastern part of the Yellow sea in spring 2017 reported by Park et al. (2018). They

https://doi.org/10.5194/acp-2020-109
Preprint. Discussion started: 16 March 2020
© Author(s) 2020. CC BY 4.0 License.

attributed the high number concentrations of particles within nucleation and Aitken modes to the long-range transport of air pollutants over eastern China under the influence of westerly winds. Consistently, larger values of N_{cn} were frequently observed in the continental atmospheres upwind of the Yellow sea, e.g., the mean values of 1.8 ± 1.4×10^4 cm^{-3} in May 2013 in Qingdao, a coastal city in proximity to the Yellow Sea (Li et al., 2015), 3.18×10^4 cm^{-3} in February-August 2014 in Beijing (Dal Maso et al., 2016), and 1.0×10^4 cm^{-3} in continental-air cases during January-December 2010 in Shanghai (Leng et al., 2013).

3.2 Spatiotemporal variations in ambient N_{ccn} during the cruise period

N_{ccn} data were generally available during the entire campaign (Fig. 3b). The mean values of N_{ccn} over China marginal seas during the DOY 110 to DOY 135, 2018 were from 3.2 ± 1.1 × 10^3 cm^{-3} to 3.9 ± 1.4 × 10^3 cm^{-3} under SS ranging from 0.2% to 1.0%(Table 1), two to four times larger than the N_{ccn} at the same SS over the NWPO in March-April 2014 (Wang et al., 2019), and much higher, i.e., 1-2 orders of magnitude, than the pristine marine background values (Quinn and Bates, 2011). As was discussed in the previous section, the mean N_{cn} in this study (8.1 ± 4.4 × 10^3 cm^{-3}) was comparable to that of N_{cn} (7.6 ± 4.0 × 10^3 cm^{-3}) over the Yellow Sea in spring 2017 in Park et al. (2018); however, the comparison of mean N_{ccn} reveals that mean value (3.6±1.2 × 10^3 cm^{-3}) at SS of 0.6% in this study was approximately 25% smaller than that (4.8 × 10^3 cm^{-3} at similar SS of 0.65%) in Park et al. (2018), likely a result of long range transport, considering the relatively distant (i.e., 500-600 km) observations away from the land depicted in Fig. 1 of Park et al., 2018, and the subsequently higher extent of aerosol aging. N_{ccn} under SS of 0.2% in this study (3.2±1.1 × 10^3) is comparable to that (3.1±1.9 × 10^3) by Li et al. (2015) in the continental atmosphere of Qingdao in May 2013, however, the increment of N_{ccn} with the increase of SS was much weaker in our study, resulting in on average of 36% smaller in N_{ccn} under SS of 0.4% to 1.0% compared to Li et al. (2015). Consistently, the sensitivity differences of N_{ccn} to SS between relatively clean (i.e., N_{cn} (8.1 ± 4.4 × 10^3) in this study) and polluted (with Ncn of 1.8 ± 1.4×10^4 cm^{-3}) environment in Li et al. (2015) is also reported by Nair et al. (2019), who found

https://doi.org/10.5194/acp-2020-109
Preprint. Discussion started: 16 March 2020
© Author(s) 2020. CC BY 4.0 License.

little sensitivity of N_{ccn} to changes in SS over the equatorial Indian Ocean (< 6 °N) with relative clean air, and much larger enhancement of N_{ccn} with the increase of SS in polluted marine atmospheres (> 6 °N).

In addition, N_{ccn} at SS from 0.1% to 1.0% during the period with high NH_4^+ (17:00 LT on DOY 114 to 10:00 LT on DOY 120) is statistically significant higher (P<0.01) in comparison to the poor NH_4^+ period (11:00 LT on DOY 120 to 7:00LT on DOY 136; Fig. 3b). More specifically, a large increase in NH_4^+ concentration, with mean concentration of 6.3±2.5 μg m^{-3}, can be observed during the period from 17:00 LT on DOY 114 to 10:00 LT on DOY 120 (Fig. 3b). The mean N_{ccn} during this period varied from $3.5 \pm 1.0\times10^3$ cm^{-3} to $4.0 \pm 1.1\times10^3$ cm^{-3} at SS ranging of 0.2% to 1.0%. In contrast, after DOY 120, the concentration of NH_4^+ (0.67±0.70 μg m^{-3}) substantially decreased by almost 90%, during which the mean N_{ccn} at each SS showed statistically significant decrease of 8% to 15%, implicative of the vital contribution to CCN of secondary ammonium salt aerosols.

Another feature depicted in Fig. 3b is the N_{ccn} during the low NH_4^+ period may even exceed the maximal value of N_{ccn} during the high NH_4^+ period. To elucidate the underlying mechanism, the N_{ccn}, under each SS, was composited and compared between the days with NH_4^+ concentration higher than the upper quartile and the days in the lower quartile, yielding some interesting findings. At SS=0.2%, the composited N_{ccn} under high NH_4^+ period was higher than that during low NH_4^+ period with statistical significance level of 0.01. There was no significant difference in N_{ccn} between the two composited periods at SS of 0.4% and 0.6%. However, the composited N_{ccn} (i.e., only selection of the upper quartile) during the high NH_4^+ period was significantly lower than the composited value during the low NH_4^+ period with P<0.01, e.g., $5.1 \pm 0.5\times10^3$ cm^{-3} versus $5.3 \pm 0.7\times10^3$ cm^{-3} at SS=0.8%, $5.2 \pm 0.5\times10^3$ cm^{-3} versus $5.7 \pm 0.7\times10^3$ cm^{-3} at SS =1.0%. During the low NH_4^+ period, the marine atmospheres over the observational zones may sometimes receive strong continental inputs and/or marine traffic emissions, leading to the larger N_{ccn}. Enhanced formation of ammonium salt

https://doi.org/10.5194/acp-2020-109
Preprint. Discussion started: 16 March 2020
© Author(s) 2020. CC BY 4.0 License.

aerosols during the high NH_4^+ period likely canceled out or even overwhelmed continental inputs and/or marine traffic emissions in increasing N_{ccn} at SS=0.2%.

In addition, fresh marine traffic emissions likely yielded a negligible contribution to N_{ccn} in the marine atmosphere because of a large amount of aged aerosols from various sources therein. For example, the mean values of N_{ccn} were 3.2×10^3 cm^{-3} and 4.5×10^3 cm^{-3} at SS=0.4% and 1.0% at 08:30-11:30 on DOY110, respectively. They were almost same as 3.2×10^3 cm^{-3} at SS=0.4% and 3.8×10^3 cm^{-3} at SS=1.0% before 06:00 on that day. The mean values of N_{cn}, however, largely increased from $6.5 \pm 0.8\times10^3$ cm^{-3} before 06:00 to $1.3\pm0.3\times10^4$ cm^{-3} at 08:30-11:30 when the ship cruised across the Yangtze River estuary (Fig. 3b).

3.3 Spatiotemporal variations in CCN activation and Kappa values

AR values at SS of 0.4% and 1.0% were examined in the section, shown in Fig. 3c. At SS=0.4%, AR values largely varied from 0.06 to 0.92 with the median value of 0.51. Specifically, AR values narrowly varied around 0.51 ± 0.04 at 00:00-06:00 LT on DOY110. At 08:00-21:00 LT on that day when the ship cruised across the Yangtze River estuary, the AR values were substantially decreased to 0.26 ± 0.06 concurrently with approximate 200% increase in N_{cn} values, i.e., N_{cn} value of $6.5 \pm 0.8\times10^3$ cm^{-3} at 00:00-06:00 LT and $2.0 \pm 0.7\times10^4$ cm^{-3} at 08:00-21:00 LT on DOY110 (Fig. 3a). The AR values then exhibited an oscillating increase from DOY 111 to DOY113. Low AR values of 0.12 ± 0.04 were suddenly observed at 10:00-18:00 LT on DOY114 in presence of strong new particle signals transported from the upwind continental atmosphere, as discussed later. AR values, however, reached 0.34± 0.04 at 06:00-08:00 LT and 0.39± 0.08 at 19:00-24:00 LT on DOY114 with the new particle signals largely reduced. Even excluding the AR values on DOY 114, a significant difference was still obtained between AR values of 0.61 ± 0.12 during the high NH_4^+ period and those of 0.55 ± 0.17 during the low NH_4^+ period. Enhanced formation of ammonium salts seemingly increased CCN activity to some extent. At SS=1.0%, AR values showed

https://doi.org/10.5194/acp-2020-109
Preprint. Discussion started: 16 March 2020
© Author(s) 2020. CC BY 4.0 License.

large fluctuation with the median value of 0.57± 0.17 (Fig. 3c) and the temporal trend was similar to that at SS=0.4%.

To minimize the impact from particle sizes, *Kappa* values were further investigated. As was reported by Phillips et al. (2018), *Kappa* values in a high time resolution usually exhibited a broad distribution, reflecting the complexity due to various of factors. To reveal the key factors in determining *Kappa* values in a large spatiotemporal scale, the daily *Kappa* values of atmospheric aerosols were estimated, on basis of the daily mean N_{ccn} and the size distributions of particle number concentration from DOY 110-118 (Fig. 3c). Please note that for DOY 110, considering large differences of particle number concentration between 00:00-06:00 and 08:00-21:00 (Fig. S1), *Kappa* values were calculated separately for these two periods. At SS=0.4% (green dashed line in Fig. 3c), the estimated *Kappa* values were as high as 0.66 at 00:00-06:00 LT while it decreased to 0.37 at 08:00-21:00 LT on DOY110. The *Kappa* value varied narrowly from 0.46 to 0.55 on DOY 111-113, 115 and 117, implying that inorganic aerosols such as completely and incompletely neutralized ammonium salts may yield a large contribution to the N_{ccn}. These values were generally consistent with reported observations in most of marine atmospheres. For example, Cai et al. (2017) reported the *Kappa* value around 0.5 for particles with sizes of 40-200 nm at a marine site in Okinawa and sulfate to be the dominant component of aerosol particles on 1-9 November 2015, and a similar *Kappa* value in spring 2008 over this site was reported by Mochida et al. (2010). Royalty et al. (2017) reported *Kappa* values for 48, 96, and 144 nm dry particles to be 0.57 ± 0.12, 0.51 ± 0.09, and 0.52 ± 0.08 in the subtropical North Pacific Ocean and sulfate-like particles contributing at most 77–88% to the total aerosol number concentration. *Kappa* values over the Atlantic Ocean were observed around 0.54 ± 0.03 for 284 nm particles (Phillips et al., 2018).

The estimated *Kappa* values sometimes reached 0.66-0.67 (i.e., on DOY 116), which may be related to unidentified factors. For example, O'Dowd et al. (2014) proposed that some organics derived from sea-spray aerosols may also increase the N_{ccn}, to some

https://doi.org/10.5194/acp-2020-109
Preprint. Discussion started: 16 March 2020
© Author(s) 2020. CC BY 4.0 License.

extent, by reducing surface intension, leading to increase of *Kappa* values. A small fraction of sea-salt aerosols in submicron particles may also increase *Kappa* values since its *Kappa* value was as high as 1.3 (O'Dowd et al., 2004; O'Dowd et al., 1997). The *Kappa* value of 0.29 was obtained on DOY118, close to *Kappa* values widely observed for continental atmospheric aerosols (~0.3) (Andreae and Rosenfeld, 2008; Poschl et al., 2009; Rose et al., 2010). The estimated *Kappa* value largely decreased to 0.15 on DOY114 when new particle formation (NPF) occurred, with detailed discussion in section 3.5. Moreover, at SS of 1.0%, the estimated *Kappa* value was always smaller than 0.2. The *Kappa* value of organics was commonly assumed as 0.1 (Cai et al., 2017; Rose et al., 2011; Singla et al., 2017). In general, the fraction of organics in nanometer particles increases with decreasing particle sizes (Cai et al., 2017; Crippa et al., 2014; Rose et al., 2011; Rose et al., 2010). A combination of the two factors likely led to overall *Kappa* values estimated at SS=1.0% to be much lower.

3.4 Particle number size distributions and CCN activation associated with marine traffic emissions and aerosol aging

The particle number size distributions during DOY 110-118, shown in Fig. 4, can be in general classified into two categories. Category 1 occurred on DOY110-114, when particle number concentrations were mainly distributed at the Aitken mode, whereas the accumulation mode was generally undetectable. Category 2 occurred on DOY115-118, when the accumulation mode can be clearly identified and generally dominated over the Aitken mode. Hoppel W. A. (1986) proposed cloud-modified aerosols to be mainly distributed at 80-150 nm in the remote tropical Atlantic and Pacific oceans. Cloud-modified aerosols are quietly common in remote marine atmosphere, likely leading to the dominate accumulation mode particles to be observed on DOY115-118. Occasionally, the Aitken mode dominated over the accumulation mode on some day such as DOY 118. To further dive into the sources of different modes of particles, three-day of DOY112, DOY 116 and DOY118 were selected.

https://doi.org/10.5194/acp-2020-109
Preprint. Discussion started: 16 March 2020
© Author(s) 2020. CC BY 4.0 License.

On DOY 112, the Aitken mode particles accounted for approximately 60% of the total particle number concentration (Fig. 5a), with median Aitken mode diameters around 54±8 nm. Like the observations over the Yangtze River estuary, the mean value of N_{cn} increased by approximately 50% concurrently with a decrease in the median Aitken mode diameters by ~9 nm at 05:30 – 11:40 LT against those at the early morning before 05:30 LT (Fig. 5b). Concomitantly, the AR values decreased to 0.31±0.09 at SS of 0.4%, with similar AR decrease at SS of 1.0%, and the lowest AR and *Kappa* values occurring at 06:00-07:00 LT at SS of both 0.4% and 1.0%. All these results pointed towards the increase in Aitken mode particles at 05:30 – 11:40 LT to be likely derived from enhanced marine traffic contributions carried by the onshore wind from the south (Fig. S10). During other time on DOY112, the onshore wind may also carry the marine-traffic derived particles to the observational sea zones. However, the marine-traffic derived particles likely aged to some extent, e.g., the median Aitken mode diameters exhibited an oscillating increase from approximately 50 nm at 19:00 to approximately 70 nm at 24:00 LT with the particle growth rate of ~4 nm $hour^{-1}$. The AR values, however, narrowly varied around 0.47±0.03 at SS=0.4% and 0.52±0.05 at SS=1.0% during the particle growth period. The *Kappa* values at SS=0.4% gradually decreased from 0.56 at 19:00 to 0.41 at 23:00 LT, reflecting more aged marine-traffic derived particles growing into CCN size.

On DOY 116, the accumulation mode particles instead of Aitken mode particles dominantly contributed to N_{cn} (Fig. 5d), under the marine air influence from the northeast (Fig. S12). The median accumulation mode diameters narrowly varied around 135±5 nm at 01:00-13:00 LT and 102±5 nm at 16:20-24:00 LT with the transition period in between (Fig. 5e). The AR and *Kappa* values, however, showed no statistically significant difference during the two periods at SS of 0.4% and 1.0%, implying that the size change in accumulation mode particles showed a negligible influence on the CCN activation. Hourly variations in AR and *Kappa* values may be associated with other factors, e.g., chemical composition, mixing state, etc. (Gunthe et al., 2011; Rose et al., 2011).

https://doi.org/10.5194/acp-2020-109
Preprint. Discussion started: 16 March 2020
© Author(s) 2020. CC BY 4.0 License.

On DOY 118, under the influence of mixture from the marine and coastal areas from the northeast (Fig. S13), the accumulation mode particles generally dominated the contribution to N_{cn} while the reverse was true in some occasions (Fig. 5g,h). The median accumulation mode diameters exhibited an oscillating increase from approximately 100 nm to 130 nm at 00:00-08:00 LT, narrowly varied around 133±5 nm at 08:00-13:00 LT, and then exhibited an oscillating decrease down to approximately 100 nm at 20:00 LT. The AR values and *Kappa* values at SS=0.4%, however, exhibited an inverted bell-shape with the lowest values at 0.31 and 0.11 at 13:00. The decreases in AR values and *Kappa* may be related to organic condensed on accumulation mode particles since the median accumulation mode diameters were almost largest at 13:00. The Aitken mode particles evidently enhanced at 14:00-15:00, but the influence on AR values and *Kappa* values at SS=0.4% was undetectable (Fig. 5i).

3.5 The long-range transport of grown new particles on DOY 114

No hour-long sharp increase in number concentration of nucleation mode particles (< 20 nm) was observed during the period from DOY 110 to DOY 118, except on DOY114 (Fig. 4). According to the conventional definition of NPF events (Dal Maso et al., 2005; Kulmala et al., 2004), the occurrence frequency of NPF events was low in this study. Unlike continental atmospheres where a high occurrence frequency of NPF events has been observed globally in spring (Kerminen et al., 2018; Kulmala et al., 2004), a low occurrence frequency reportedly occurred over the seas during the "Meiyu (plum-rain) season" in spring because of frequent rainy, foggy or cloudy weather conditions (Zhu et al., 2019). Lack of NPF events in the marine atmospheres implied N_{cn} and N_{ccn} to be mainly contributed by primarily emitted aerosols and their aged products.

During the period of 10:00-18:00 LT on DOY 114, a large increase in number concentrations of Aitken mode particles (Fig. 6a) likely reflected the long-range transport of grown new particles from upwind continental atmospheres (Fig. S11). The size distributions of particle number concentration showed a dominant Aitken mode at

https://doi.org/10.5194/acp-2020-109
Preprint. Discussion started: 16 March 2020
© Author(s) 2020. CC BY 4.0 License.

10:00-18:00 LT, when spatiotemporal variations in N_{cn} and median Aitken mode diameters exhibited bell-shape patterns (Fig. 6b). The median Aitken mode diameters increased from 26 nm at 10:00 LT to 33 nm at 12:00-13:00 LT and then decreased to 20 nm prior to the signal disappeared, likely reflecting the growth and shrinkage of the Aitken mode particles (Yao et al., 2010; Zhu et al., 2019). The median Aitken mode diameters were evidently smaller than the values, i.e., 40-50 nm for Aitken mode particles, observed over the Yangtze River estuary on DOY 112 (Fig. 5a). Moreover, the number concentrations of 20-40 nm particles increased by 5.8 times at 12:00-13:00 LT compared to the mean value at 06:00-09:00 LT while the total number concentrations of particles greater than 90 nm increased by only 67%. These results implied the largely increased number concentrations of Aitken mode particles with a dynamic change in mode diameter observed at 10:00-18:00 LT unlikely to be caused by primarily emitted and aged particles from marine traffic emissions or other combustion sources. The observations of gaseous and particulate species, during the same period, implied air masses to be well-aged and less polluted. For instance, the measured hourly average mixing ratios of SO_2 was no larger than 1.2 ppb (Fig. 6c) and the hourly average concentrations of NH_4^+ in $PM_{2.5}$ were smaller than 2 μg m^{-3} (Fig. 3b). In addition, the concentrations of K^+ were below 0.3 μg m^{-3}, suggesting negligible contributions from biomass burning (Fig. 6e).

Before 09:00 LT, a much weaker spike of nucleation mode particles was intermittently observed (Fig. 6a). The weak and intermittent NPF seems to occur in the marine atmospheres before 09:00 LT when no apparent growth of new particles was observed. Possibly due to the transport from the continent (Fig. S11) and an increase in the condensational sink around 10:00 am (Fig. 6a), the weak NPF signal gradually dropped to a negligible level half an hour later, concomitant with a large increase in the number concentrations of Aitken mode particles at 10:00-18:00 LT.

N_{ccn} at SS=0.4% increased from 1.2×10^3 cm^{-3} at 06:00-09:00 LT to the peak value of

https://doi.org/10.5194/acp-2020-109
Preprint. Discussion started: 16 March 2020
© Author(s) 2020. CC BY 4.0 License.

2.3×10^3 cm^{-3} at 12:00 LT, with increase of 92%, and N_{ccn} at SS=1.0% increased from 1.6×10^3 cm^{-3} to 4.0×10^3 cm^{-3}, with increase of 150% (Fig. 6d). The net increase in N_{ccn} at SS=0.4% likely reflected the contribution from pre-existing particles since new particles with the diameter less than 50 nm were unlikely activated as CCN at such low SS (Li et al., 2015; Ma et al., 2016; Wu et al., 2016). The larger net increase in N_{ccn} at SS=1.0% may reflect the contributions mixed from pre-existing particles and grown new particles. The high SS can activate particles as CCN with diameters down 40 nm (Dusek et al., 2006; Li et al., 2015). The invasion of grown new particles also led to the AR values largely decreased from 0.3 to 0.1 at SS=0.4%, and from 0.4 to 0.2 at SS=1.0% (Fig. 6e). After 18:00 LT, the AR values retuned to 0.3-0.4 at SS=0.4% and 0.4-0.6 at SS=1.0%. When the calculated *Kappa* values were examined (Fig. 6c), they decreased from 0.4 to 0.1-0.2 at SS=0.4%. The value returned to 0.3 at 18:00-19:00 LT (FMPS was temporarily malfunctioned after 19:20 LT). The *Kappa* values were below 0.2 at SS=1.0% on that day. The decreases in AR values and *Kappa* values at two SS were likely caused by organic vapor condensed on preexisting particles and new particles (Wu et al., 2016; Zhu et al., 2019).

3.6 Correlations of N_{cn} and N_{ccn} with SO_2 in self-ship plumes and ambient air

When self-ship emission signals were detected, the observational values included a combination of contributions from self-ship emissions and ambient concentrations. Although ambient N_{cn} was negligible in comparison with N_{cn} derived from self-ship emissions, it was not the case for N_{ccn} and SO_2. Based on the minutely data, the signal was considered as vessel-self emission when both N_{cn} greater than 50,000 cm^{-3} and SO_2 greater than 5 ppb. The composited data was then used to derive the hourly average N_{cn}, N_{ccn} and SO_2, which was then subtracted by the ambient hourly mean value during the preceding hour with relatively clean conditions (i.e., concentration of N_{cn} lower than 10,000 cm^{-3}, SO_2 lower than 2.5 ppb). Please note uncertainties exist in terms of the criteria and separation between self-ship and ambient signals, however, minimal impact is expected in the relationship examined below.

https://doi.org/10.5194/acp-2020-109
Preprint. Discussion started: 16 March 2020
© Author(s) 2020. CC BY 4.0 License.

Fig. 7a showed correlations of N_{cn} and N_{ccn} with mixing ratio of SO_2 in self-ship plumes, prefixed by Δ for N_{cn}, N_{ccn} and SO_2 to implicate the removal of ambient signals. . A good correlation of 0.66 for R^2 ($P<0.01$) was obtained and the slope indicates that N_{cn} increase by 1.4×10^4 cm^{-3} for each ppb increase of SO_2 resulted from ship emission (Fig. 7a). High emissions of N_{cn} were generally reported in engine exhausts with high sulfur-content diesel to be used (Yao et al., 2007; Yao et al., 2005). In regard of N_{ccn} at SS of 0.2% to 1.0% (Fig. 7b), it increases from 30 cm^{-3} to 170 cm^{-3} per 1 ppb increase of SO_2, showing statistical significant correlation at 99th confidence level. The contribution ratio of SO_2 to N_{ccn} is 0.002 (SS of 0.2%), 0.004(SS of 0.4%) and 0.012 (SS of 1.0%) to that of N_{cn}, in general consistent with the previous study by Ramana and Devi (2016), in which a range of 0.0012–0.57 was observed for CCN at 0.4% in Bay of Bengal during Aug 13–16, 2012.

The correlations of hourly averaged N_{cn} and N_{ccn} with SO_2 in ambient air were examined and showed in Fig. 7c,d. The data was segmented into pieces based on SO_2 with interval of 0.2 ppb. A good correlation between the averaged N_{cn} and SO_2 were obtained with R^2 of 0.80 ($P<0.01$) and 1 ppb increase in SO_2 likely increased N_{cn} by 1.6×10^3 cm^{-3} (Fig. 7c). The increase in N_{cn} with SO_2 may reflect the contribution from primary emissions. An intercept was, however, as large as 3.9×10^3 cm^{-3}, likely representing the contribution from well-aged aerosols.

Hourly averaged N_{ccn} at different SS generally increased with increase of ambient SO_2 (Fig. 7d). A good correlation between the averaged N_{ccn} and SO_2 were obtained with R^2=0.78-0.91 ($P<0.01$). 1 ppb increase in SO_2 likely increased N_{ccn} by 0.6×10^3 to 0.8×10^3 cm^{-3} at SS from 0.2% to 1.0%. The increase in N_{ccn} with SO_2 may also reflect the contribution from primary emissions. The intercepts of 2.2×10^3-2.7×10^3 cm^{-3} at different SS were likely contributed by well-aged aerosols. The relationship may be used as an estimation of N_{ccn} in marine atmospheres over China marginal seas, when no measurements of CCN were available whereas ambient SO_2 can be estimated from

https://doi.org/10.5194/acp-2020-109
Preprint. Discussion started: 16 March 2020
© Author(s) 2020. CC BY 4.0 License.

web-based satellite data.

4. Conclusions

Spatiotemporal variations in ambient N_{cn} and N_{ccn} were studied during a cruise campaign on DOY 110-135 over China marginal seas. The mean values of N_{cn} (8.1×10^3 cm^{-3}) and N_{ccn} at SS of 0.2%-1.0% (3.2 -3.9 $\times10^3$ cm^{-3}) were approximately one order of magnitude larger than those in remote clear marine atmospheres, indicating overwhelming contributions from non-sea-spray aerosols such as marine traffic emissions, the long-range continental transport and others.

Observed self-ship emission signals showed fresh marine traffic emissions can be important sources of N_{cn}, but a minor source of N_{ccn} in the marine atmosphere. The signals showed that 1 ppb increase in SO_2 corresponds to 1.4×10^4 cm^{-3} increase in N_{cn} and 30-170 cm^{-3} increase in N_{ccn} at SS=0.2-1.0%. Data analysis showed that marine traffic emissions largely increased N_{cn} over their heavily travelled sea zones in daytime.

In ambient marine air, the growth of marine traffic derived particles led to a decrease in estimated bulk kappa values at 0.4% possibly because some of these particles enriched in organics grew into CCN size. However, strong formation of ammonium salts led to aerosol aging, and significantly increased N_{ccn} at SS of 0.2-1.0% in comparison with those observed during the period poor in ammonium salt aerosols in $PM_{2.5}$ with $P<0.01$. The estimated bulk *Kappa* values from the daily average values varied from 0.46 to 0.55 at SS=0.4% in most of marine atmospheres, indicating inorganic ammonium aerosols may dominantly contribute to the N_{ccn} at SS of 0.4%. The particle number size distributions showed the high bulk *Kappa* values could be related to cloud-modified aerosols, which likely led to a large extent of degradation of organics and subsequently lost from the particle phase.

Humid marine ambient air led to NPF events rarely occurring therein. The dominant

https://doi.org/10.5194/acp-2020-109
Preprint. Discussion started: 16 March 2020
© Author(s) 2020. CC BY 4.0 License.

onshore winds occurred most of the measurement periods, and should carry primary aerosols and their aged products rather than secondarily formed aerosols to the observational zone. During an occasion when offshore winds blew from the northwest (Fig. S11), new particle signals transported from the continent can be clearly observed. However, NPF in the marine atmosphere was too weak to be important. The transported new particles from the continent yielded the maximal increase in N_{ccn} by 92% at SS of 0.4% and 150% at SS of 1.0%. However, consistent with those reported in literature, the estimated *kappa* values largely decreased from 0.4 to 0.1-0.2 at SS=0.4% during most time of the continent-transported NPF event because of the *kappa* value of organic condensation vapor as low as 0.1.

Competing interests. The authors declare that they have no conflict of interest.

Author contributions. YG and XY designed the research, YG, DZ and XY performed the analysis, JW and HG helped on the interpretation of the results, and all co-authors contributed to the writing of the paper.

Acknowledgment

This research is supported by the National Key Research and Development Program in China (grant no. 2016YFC0200504) and the Natural Science Foundation of China (grant no. 41576118).

References

Andreae, M. O., and Rosenfeld, D.: Aerosol-cloud-precipitation interactions. Part 1. The nature and sources of cloud-active aerosols, Earth-Sci. Rev., 89, 13-41, 10.1016/j.earscirev.2008.03.001, 2008.

Blot, R., Clarke, A. D., Freitag, S., Kapustin, V., Howell, S. G., Jensen, J. B., Shank, L. M., McNaughton, C. S., and Brekhovskikh, V.: Ultrafine sea spray aerosol over the southeastern Pacific: open-ocean contributions to marine boundary layer CCN, Atmos. Chem. Phys., 13, 7263-7278, 10.5194/acp-13-7263-2013, 2013.

Bougiatioti, A., Fountoukis, C., Kalivitis, N., Pandis, S. N., Nenes, A., and Mihalopoulos,

https://doi.org/10.5194/acp-2020-109
Preprint. Discussion started: 16 March 2020
© Author(s) 2020. CC BY 4.0 License.

N.: Cloud condensation nuclei measurements in the eastern Mediterranean marine boundary layer: CCN closure and droplet growth kinetics, Atmos. Chem. Phys.Discuss., 9, 10303-10336, 10.5194/acpd-9-10303-2009, 2009.

Brooks, S. D., and Thornton, D. C. O.: Marine Aerosols and Clouds, Annu. Rev. Mar. Sci., 10, 289-313, 10.1146/annurev-marine-121916-063148, 2018.

Cai, M. F., Tan, H. B., Chan, C. K., Mochida, M., Hatakeyama, S., Kondo, Y., Schurman, M. I., Xu, H. B., Li, F., Shimada, K., Li, L., Deng, Y. G., Yai, H., Matsuki, A., Qin, Y. M., and Zhao, J.: Comparison of Aerosol Hygroscopcity, Volatility, and Chemical Composition between a Suburban Site in the Pearl River Delta Region and a Marine Site in Okinawa, Aerosol. Air. Qual. Res., 17, 3194-3208, 10.4209/aaqr.2017.01.0020, 2017.

Charlson, R. J., Lovelock, J. E., Andreae, M. O., and Warren, S. G.: Oceanic phytoplankton atmospheric sulpher cloud albedo and climate, Nature, 326, 655-661, 1987.

Chen, D. S., Wang, X. T., Li, Y., Lang, J. L., Zhou, Y., Guo, X. R., and Zhao, Y. H.: High-spatiotemporal-resolution ship emission inventory of China based on AIS data in 2014, Sci. Total Environ., 609, 776-787, 10.1016/j.scitotenv.2017.07.051, 2017a.

Chen, J. M., Li, C. L., Ristovski, Z., Milic, A., Gu, Y. T., Islam, M. S., Wang, S. X., Hao, J. M., Zhang, H. F., He, C. R., Guo, H., Fu, H. B., Miljevic, B., Morawska, L., Thai, P., Fat, L. A. M. Y., Pereira, G., Ding, A. J., Huang, X., and Dumka, U. C.: A review of biomass burning: Emissions and impacts on air quality, health and climate in China, Sci. Total Environ., 579, 1000-1034, 10.1016/j.scitotenv.2016.11.025, 2017b.

Clarke, A. D., Owens, S. R., and Zhou, J. C.: An ultrafine sea-salt flux from breaking waves: Implications for cloud condensation nuclei in the remote marine atmosphere, J. Geophys. Res.-Atmos., 111, Artn D06202,10.1029/2005jd006565, 2006.

Crippa, M., Canonaco, F., Lanz, V. A., Aijala, M., Allan, J. D., Carbone, S., Capes, G., Ceburnis, D., Dall'Osto, M., Day, D. A., DeCarlo, P. F., Ehn, M., Eriksson, A., Freney, E., Hildebrandt Ruiz, L., Hillamo, R., Jimenez, J. L., Junninen, H., Kiendler-Scharr, A., Kortelainen, A. M., Kulmala, M., Laaksonen, A., Mensah, A., Mohr, C., Nemitz, E., O'Dowd, C., Ovadnevaite, J., Pandis, S. N., Petaja, T., Poulain, L., Saarikoski, S.,

https://doi.org/10.5194/acp-2020-109
Preprint. Discussion started: 16 March 2020
© Author(s) 2020. CC BY 4.0 License.

Sellegri, K., Swietlicki, E., Tiitta, P., Worsnop, D. R., Baltensperger, U., and Prevot, A. S. H.: Organic aerosol components derived from 25 AMS data sets across Europe using a consistent ME-2 based source apportionment approach, Atmos. Chem. Phys., 14, 6159-6176, 10.5194/acp-14-6159-2014, 2014.

Dal Maso, M., Kulmala, M., Riipinen, I., Wagner, R., Hussein, T., Aalto, P. P., and Lehtinen, K. E. J.: Formation and growth of fresh atmospheric aerosols: eight years of aerosol size distribution data from SMEAR II, Hyytiala, Finland, Boreal Environ. Res., 10, 323-336, 2005.

Dal Maso, M., Gao, J., Jarvinen, A., Li, H., Luo, D. T., Janka, K., and Ronkko, T.: Improving Urban Air Quality Measurements by a Diffusion Charger Based Electrical Particle Sensors - A Field Study in Beijing, China, Aerosol. Air. Qual. Res., 16, 3001-3011, 10.4209/aaqr.2015.09.0546, 2016.

Decesari, S., Finessi, E., Rinaldi, M., Paglione, M., Fuzzi, S., Stephanou, E. G., Tziaras, T., Spyros, A., Ceburnis, D., O'Dowd, C., Dall'Osto, M., Harrison, R. M., Allan, J., Coe, H., and Facchini, M. C.: Primary and secondary marine organic aerosols over the North Atlantic Ocean during the MAP experiment, J. Geophys. Res.-Atmos., 116, Artn D22210,10.1029/2011jd016204, 2011.

Ding, X., Qi, J. H., and Meng, X. B.: Characteristics and sources of organic carbon in coastal and marine atmospheric particulates over East China, Atmos. Res., 228, 281-291, 10.1016/j.atmosres.2019.06.015, 2019.

Dusek, U., Frank, G. P., Hildebrandt, L., Curtius, J., Schneider, J., Walter, S., Chand, D., Drewnick, F., Hings, S., Jung, D., Borrmann, S., and Andreae, M. O.: Size matters more than chemistry for cloud-nucleating ability of aerosol particles, Science, 312, 1375-1378, 10.1126/science.1125261, 2006.

Feng, J. L., Guo, Z. G., Zhang, T. R., Yao, X. H., Chan, C. K., and Fang, M.: Source and formation of secondary particulate matter in PM2.5 in Asian continental outflow, J. Geophys. Res.-Atmos., 117, Artn D03302,10.1029/2011jd016400, 2012.

Feng, L., Shen, H., Zhu, Y., Gao, H., and Yao, X.: Insight into Generation and Evolution of Sea-Salt Aerosols from Field Measurements in Diversified Marine and Coastal Atmospheres, Sci. Rep., 7, 41260, 10.1038/srep41260, 2017.

https://doi.org/10.5194/acp-2020-109
Preprint. Discussion started: 16 March 2020
© Author(s) 2020. CC BY 4.0 License.

Feng, T., Li, G. H., Cao, J. J., Bei, N. F., Shen, Z. X., Zhou, W. J., Liu, S. X., Zhang, T., Wang, Y. C., Huang, R. J., Tie, X. X., and Molina, L. T.: Simulations of organic aerosol concentrations during springtime in the Guanzhong Basin, China, Atmos. Chem. Phys., 16, 10045-10061, 10.5194/acp-16-10045-2016, 2016.

Fossum, K. N., Ovadnevaite, J., Ceburnis, D., Dall'Osto, M., Marullo, S., Bellacicco, M., Simo, R., Liu, D. T., Flynn, M., Zuend, A., and O'Dowd, C.: Summertime Primary and Secondary Contributions to Southern Ocean Cloud Condensation Nuclei, Sci. Rep., 8, Artn 13844,10.1038/S41598-018-32047-4, 2018.

Fu, X. G., Wang, M., Zeng, S. Q., Feng, X. L., Wang, D., and Song, C. Y.: Continental weathering and palaeoclimatic changes through the onset of the Early Toarcian oceanic anoxic event in the Qiangtang Basin, eastern Tethys, Palaeogeogr. Palaeocl., 487, 241-250, 10.1016/j.palaeo.2017.09.005, 2017.

Gunthe, S. S., Rose, D., Su, H., Garland, R. M., Achtert, P., Nowak, A., Wiedensohler, A., Kuwata, M., Takegawa, N., Kondo, Y., Hu, M., Shao, M., Zhu, T., Andreae, M. O., and Pöschl, U.: Cloud condensation nuclei (CCN) from fresh and aged air pollution in the megacity region of Beijing, Atmos. Chem. Phys., 11, 11023-11039, 10.5194/acp-11-11023-2011, 2011.

Guo, L., Chen, Y., Wang, F., Meng, X., Xu, Z., and Zhuang, G.: Effects of Asian dust on the atmospheric input of trace elements to the East China Sea, Mar. Chem., 163, 19-27, 10.1016/j.marchem.2014.04.003, 2014.

Guo, T., Li, K., Zhu, Y., Gao, H., and Yao, X.: Concentration and size distribution of particulate oxalate in marine and coastal atmospheres – Implication for the increased importance of oxalate in nanometer atmospheric particles, Atmos. Environ., 142, 19-31, 10.1016/j.atmosenv.2016.07.026, 2016.

Hoppel W. A., F. G. M., and Larson R. E.: Effect of non-precipitating clouds on the aerosol size distribution, Geophys. Res. Lett., 13, 125-128, 1986.

Huebert, B. J., Bates, T., Russell, P. B., Shi, G. Y., Kim, Y. J., Kawamura, K., Carmichael, G., and Nakajima, T.: An overview of ACE-Asia: Strategies for quantifying the relationships between Asian aerosols and their climatic impacts, J. Geophys. Res.-Atmos., 108, Artn 8633,10.1029/2003jd003550, 2003.

https://doi.org/10.5194/acp-2020-109
Preprint. Discussion started: 16 March 2020
© Author(s) 2020. CC BY 4.0 License.

Kerminen, V. M., Chen, X. M., Vakkari, V., Petaja, T., Kulmala, M., and Bianchi, F.: Atmospheric new particle formation and growth: review of field observations, Environ. Res. Lett., 13, Artn 103003,10.1088/1748-9326/Aadf3c, 2018.

Kulmala, M., Vehkamaki, H., Petaja, T., Dal Maso, M., Lauri, A., Kerminen, V. M., Birmili, W., and McMurry, P. H.: Formation and growth rates of ultrafine atmospheric particles: a review of observations, J. Aer. Sci., 35, 143-176, 10.1016/j.jaerosci.2003.10.003, 2004.

Langley, L., Leaitch, W. R., Lohmann, U., Shantz, N. C., and Worsnop, D. R.: Contributions from DMS and ship emissions to CCN observed over the summertime North Pacific, Atmos. Chem. Phys., 10, 1287-1314, DOI 10.5194/acp-10-1287-2010, 2010.

Leng, C., Cheng, T., Chen, J., Zhang, R., Tao, J., Huang, G., Zha, S., Zhang, M., Fang, W., Li, X., and Li, L.: Measurements of surface cloud condensation nuclei and aerosol activity in downtown Shanghai, Atmos. Environ., 69, 354-361, 10.1016/j.atmosenv.2012.12.021, 2013.

Li, K., Zhu, Y., Gao, H., and Yao, X.: A comparative study of cloud condensation nuclei measured between non-heating and heating periods at a suburb site of Qingdao in the North China, Atmos. Environ., 112, 40-53, 10.1016/j.atmosenv.2015.04.024, 2015.

Li, M., Liu, H., Geng, G., Hong, C., Liu, F., Song, Y., Tong, D., Zheng, B., Cui, H., Man, H., Zhang, Q., and He, K.: Anthropogenic emission inventories in China: a review, Natl. Sci. Rev., 4, 834-866, 10.1093/nsr/nwx150, 2017.

Lin, Y. C., Chen, J. P., Ho, T. Y., and Tsai, I. C.: Atmospheric iron deposition in the northwestern Pacific Ocean and its adjacent marginal seas: The importance of coal burning, Global. Biogeochem. Cy., 29, 138-159, 10.1002/2013GB004795, 2015.

Liu, F., Zhang, Q., A., R. J. v. d., Zheng, B., Tong, D., Yan, L., Zheng, Y., and He, K.: Recent reduction in NO x emissions over China: synthesis of satellite observations and emission inventories, Environ. Res. Lett., 11, 114002, 2016.

Ma, N., Zhao, C. S., Tao, J. C., Wu, Z. J., Kecorius, S., Wang, Z. B., Gross, J., Liu, H. J., Bian, Y. X., Kuang, Y., Teich, M., Spindler, G., Muller, K., van Pinxteren, D., Herrmann, H., Hu, M., and Wiedensohler, A.: Variation of CCN activity during new

https://doi.org/10.5194/acp-2020-109
Preprint. Discussion started: 16 March 2020
© Author(s) 2020. CC BY 4.0 License.

particle formation events in the North China Plain, Atmos. Chem. Phys., 16, 8593-8607, 10.5194/acp-16-8593-2016, 2016.

Mochida, M., Nishita-Hara, C., Kitamori, Y., Aggarwal, S. G., Kawamura, K., Miura, K., and Takami, A.: Size-segregated measurements of cloud condensation nucleus activity and hygroscopic growth for aerosols at Cape Hedo, Japan, in spring 2008, J. Geophys. Res., 115, 10.1029/2009jd013216, 2010.

Nair, V. S., Nair, J. V., Kompalli, S. K., Gogoi, M. M., and Babu, S. S.: Cloud Condensation Nuclei properties of South Asian outflow over the northern Indian Ocean during winter, Atmos. Chem. Phys.Discuss., 10.5194/acp-2019-828, 2019.

O'Dowd, C., Ceburnis, D., Ovadnevaite, J., Vaishya, A., Rinaldi, M., and Facchini, M. C.: Do anthropogenic, continental or coastal aerosol sources impact on a marine aerosol signature at Mace Head?, Atmos. Chem. Phys., 14, 10687-10704, 10.5194/acp-14-10687-2014, 2014.

O'Dowd, C. D., Smith, M. H., Consterdine, I. E., and Lowe, J. A.: Marine aerosol, sea-salt, and the marine sulphur cycle: A short review, Atmos. Environ., 31, 73-80, Doi 10.1016/S1352-2310(96)00106-9, 1997.

O'Dowd, C. D., Facchini, M. C., Cavalli, F., Ceburnis, D., Mircea, M., Decesari, S., Fuzzi, S., Yoon, Y. J., and Putaud, J. P.: Biogenically driven organic contribution to marine aerosol, Nature, 431, 676-680, 10.1038/nature02959, 2004.

Park, M., Yum, S. S., Kim, N., Cha, J. W., Shin, B., and Ryoo, S.-B.: Characterization of submicron aerosols and CCN over the Yellow Sea measured onboard the Gisang 1 research vessel using the positive matrix factorization analysis method, Atmos. Res., 214, 430-441, 10.1016/j.atmosres.2018.08.015, 2018.

Petters, M. D., and Kreidenweis, S. M.: A single parameter representation of hygroscopic growth and cloud condensation nucleus activity, Atmos. Chem. Phys., 7, 1961-1971, DOI 10.5194/acp-7-1961-2007, 2007.

Phillips, B. N., Royalty, T. M., Dawson, K. W., Reed, R., Petters, M. D., and Meskhidze, N.: Hygroscopicity- and Size-Resolved Measurements of Submicron Aerosol on the East Coast of the United States, J. Geophys. Res.-Atmos., 123, 1826-1839, 10.1002/2017JD027702, 2018.

https://doi.org/10.5194/acp-2020-109
Preprint. Discussion started: 16 March 2020
© Author(s) 2020. CC BY 4.0 License.

Pöschl, U., Rose, D., & Andreae, M. O. (2009). Climatologies of Cloud-related Aerosols. Part 2: Particle Hygroscopicity and Cloud Condensation Nucleus Activity. In J. Heintzenberg, & R. J. Charlson (Eds.), Clouds in the Perturbed Climate System: Their Relationship to Energy Balance, Atmospheric Dynamics, and Precipitation (pp. 58-72). Cambridge: MIT Press.

Quinn, P. K., and Bates, T. S.: The case against climate regulation via oceanic phytoplankton sulphur emissions, Nature, 480, 51-56, 10.1038/nature10580, 2011.

Quinn, P. K., Collins, D. B., Grassian, V. H., Prather, K. A., and Bates, T. S.: Chemistry and Related Properties of Freshly Emitted Sea Spray Aerosol, Chem. Rev., 115, 4383-4399, 10.1021/cr500713g, 2015.

Ramana, M. V., and Devi, A.: CCN concentrations and BC warming influenced by maritime ship emitted aerosol plumes over southern Bay of Bengal, Sci. Rep., 6, 30416, 10.1038/srep30416, 2016.

Rose, D., Gunthe, S. S., Mikhailov, E., Frank, G. P., Dusek, U., Andreae, M. O., and Pöschl, U.: Calibration and measurement uncertainties of a continuous-flow cloud condensation nuclei counter (DMT-CCNC): CCN activation of ammonium sulfate and sodium chloride aerosol particles in theory and experiment, Atmos. Chem. Phys., 8, 1153–1179, https://doi.org/10.5194/acp-8-1153-2008, 2008.

Rose, D., Nowak, A., Achtert, P., Wiedensohler, A., Hu, M., Shao, M., Zhang, Y., Andreae, M. O., and Pöschl, U.: Cloud condensation nuclei in polluted air and biomass burning smoke near the mega-city Guangzhou, China - Part 1: Size-resolved measurements and implications for the modeling of aerosol particle hygroscopicity and CCN activity, Atmos. Chem. Phys., 10, 3365-3383, DOI 10.5194/acp-10-3365-2010, 2010.

Rose, D., Gunthe, S. S., Su, H., Garland, R. M., Yang, H., Berghof, M., Cheng, Y. F., Wehner, B., Achtert, P., Nowak, A., Wiedensohler, A., Takegawa, N., Kondo, Y., Hu, M., Zhang, Y., Andreae, M. O., and Pöschl, U.: Cloud condensation nuclei in polluted air and biomass burning smoke near the mega-city Guangzhou, China – Part 2: Size-resolved aerosol chemical composition, diurnal cycles, and externally mixed weakly CCN-active soot particles, Atmos. Chem. Phys., 11, 2817-2836, 10.5194/acp-11-

https://doi.org/10.5194/acp-2020-109
Preprint. Discussion started: 16 March 2020
© Author(s) 2020. CC BY 4.0 License.

2817-2011, 2011.

Rosenfeld, D., Zhu, Y. N., Wang, M. H., Zheng, Y. T., Goren, T., and Yu, S. C.: Aerosol-driven droplet concentrations dominate coverage and water of oceanic low-level clouds, Science, 363, 10.1126/science.aav0566, 2019.

Royalty, T. M., Phillips, B. N., Dawson, K. W., Reed, R., Meskhidze, N., and Petters, M. D.: Aerosol Properties Observed in the Subtropical North Pacific Boundary Layer, J. Geophys. Res.-Atmos., 122, 9990-10012, 10.1002/2017JD026897, 2017.

Ruehl, C. R., Chuang, P. Y., and Nenes, A.: Distinct CCN activation kinetics above the marine boundary layer along the California coast, Geophys. Res. Lett., 36, L15814, 10.1029/2009gl038839, 2009.

Saliba, G., Chen, C. L., Lewis, S., Russell, L. M., Rivellini, L. H., Lee, A. K. Y., Quinn, P. K., Bates, T. S., Haentjens, N., Boss, E. S., Karp-Boss, L., Baetge, N., Carlson, C. A., and Behrenfeld, M. J.: Factors driving the seasonal and hourly variability of sea-spray aerosol number in the North Atlantic, Proc. Natl. Acad. Sci. U.S.A., 116, 20309-20314, 10.1073/pnas.1907574116, 2019.

Sato, Y., and Suzuki, K.: How do aerosols affect cloudiness?, Science, 363, 580-581, 10.1126/science.aaw3720, 2019.

Si, Y. D., Yu, C., Zhang, L., Zhu, W. D., Cai, K., Cheng, L. X., Chen, L., and Li, S. S.: Assessment of satellite-estimated near-surface sulfate and nitrate concentrations and their precursor emissions over China from 2006 to 2014, Sci. Total Environ., 669, 362-376, 10.1016/j.scitotenv.2019.02.180, 2019.

Singla, V., Mukherjee, S., Safai, P. D., Meena, G. S., Dani, K. K., and Pandithurai, G.: Role of organic aerosols in CCN activation and closure over a rural background site in Western Ghats, India, Atmos. Environ., 158, 148-159, 10.1016/j.atmosenv.2017.03.037, 2017.

Song, J. W., Zhao, Y., Zhang, Y. Y., Fu, P. Q., Zheng, L. S., Yuan, Q., Wang, S., Huang, X. F., Xu, W. H., Cao, Z. X., Gromov, S., and Lai, S. C.: Influence of biomass burning on atmospheric aerosols over the western South China Sea: Insights from ions, carbonaceous fractions and stable carbon isotope ratios, Environ. Pollut., 242, 1800-1809, 10.1016/j.envpol.2018.07.088, 2018.

https://doi.org/10.5194/acp-2020-109
Preprint. Discussion started: 16 March 2020
© Author(s) 2020. CC BY 4.0 License.

Ueda, S., Miura, K., Kawata, R., Furutani, H., Uematsu, M., Omori, Y., and Tanimoto, H.: Number-size distribution of aerosol particles and new particle formation events in tropical and subtropical Pacific Oceans, Atmos. Environ., 142, 324-339, 10.1016/j.atmosenv.2016.07.055, 2016.

Wang, J., Shen, Y., Li, K., Gao, Y., Gao, H., and Yao, X.: Nucleation-mode particle pool and large increases in Ncn and Nccn observed over the northwestern Pacific Ocean in the spring of 2014, Atmos. Chem. Phys., 19, 8845-8861, 10.5194/acp-19-8845-2019, 2019.

Wang, Z. J., Du, L. B., Li, X. X., Meng, X. Q., Chen, C., Qu, J. L., Wang, X. F., Liu, X. T., and Kabanov, V. V.: Observations of marine aerosol by a shipborne multiwavelength lidar over the Yellow Sea of China, Lidar Remote Sensing for Environmental Monitoring Xiv.International Society for Optics and Photonics, 9262, 10.1117/12.2070297, 2014.

Wu, Z. J., Zheng, J., Shang, D. J., Du, Z. F., Wu, Y. S., Zeng, L. M., Wiedensohler, A., and Hu, M.: Particle hygroscopicity and its link to chemical composition in the urban atmosphere of Beijing, China, during summertime, Atmos. Chem. Phys., 16, 1123-1138, 10.5194/acp-16-1123-2016, 2016.

Yamashita, K., Murakami, M., Hashimoto, A., and Tajiri, T.: CCN Ability of Asian Mineral Dust Particles and Their Effects on Cloud Droplet Formation, J. Meteor. Soc. Japan, 89, 581-587, 10.2151/jmsj.2011-512, 2011.

Yao, X. H., Lau, N. T., Fang, M., and Chan, C. K.: Real-time observation of the transformation of ultrafine atmospheric particle modes, Aerosol. Sci. Tech., 39, 831-841, 10.1080/02786820500295248, 2005.

Yao, X. H., Lau, N. T., Chan, C. K., and Fang, M.: Size distributions and condensation growth of submicron particles in on-road vehicle plumes in Hong Kong, Atmos. Environ., 41, 3328-3338, 10.1016/j.atmosenv.2006.12.044, 2007.

Yao, X. H., Choi, M. Y., Lau, N. T., Lau, A. P. S., Chan, C. K., and Fang, M.: Growth and Shrinkage of New Particles in the Atmosphere in Hong Kong, Aerosol. Sci. Tech., 44, 639-650, Pii 924397031,10.1080/02786826.2010.482576, 2010.

Yu, F., and Luo, G.: Simulation of particle size distribution with a global aerosol model:

https://doi.org/10.5194/acp-2020-109
Preprint. Discussion started: 16 March 2020
© Author(s) 2020. CC BY 4.0 License.

contribution of nucleation to aerosol and CCN number concentrations, Atmos. Chem. Phys., 9, 7691-7710, DOI 10.5194/acp-9-7691-2009, 2009.

Zhu, Y. J., Li, K., Shen, Y. J., Gao, Y., Liu, X. H., Yu, Y., Gao, H. W., and Yao, X. H.: New particle formation in the marine atmosphere during seven cruise campaigns, Atmos. Chem. Phys., 19, 89-113, 10.5194/acp-19-89-2019, 2019.

Zimmerman, N., Jeong, C.-H., Wang, J. M., Ramos, M., Wallace, J. S., and Evans, G. J.: A source-independent empirical correction procedure for the fast mobility and engine exhaust particle sizers, Atmos. Environ., 100, 178-184, 10.1016/j.atmosenv.2014.10.054, 2015.

https://doi.org/10.5194/acp-2020-109
Preprint. Discussion started: 16 March 2020
© Author(s) 2020. CC BY 4.0 License.

Atmospheric Chemistry and Physics
Discussions

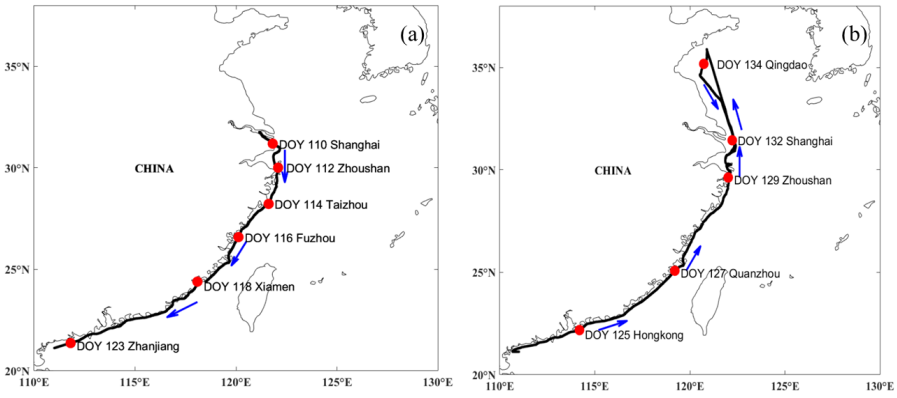

Fig 1 The ship track during the campaign of 2018, and the blue arrows represented the sailing direction, with southward track (a) and northward track (b).

https://doi.org/10.5194/acp-2020-109
Preprint. Discussion started: 16 March 2020
© Author(s) 2020. CC BY 4.0 License.

Atmospheric Chemistry and Physics Discussions

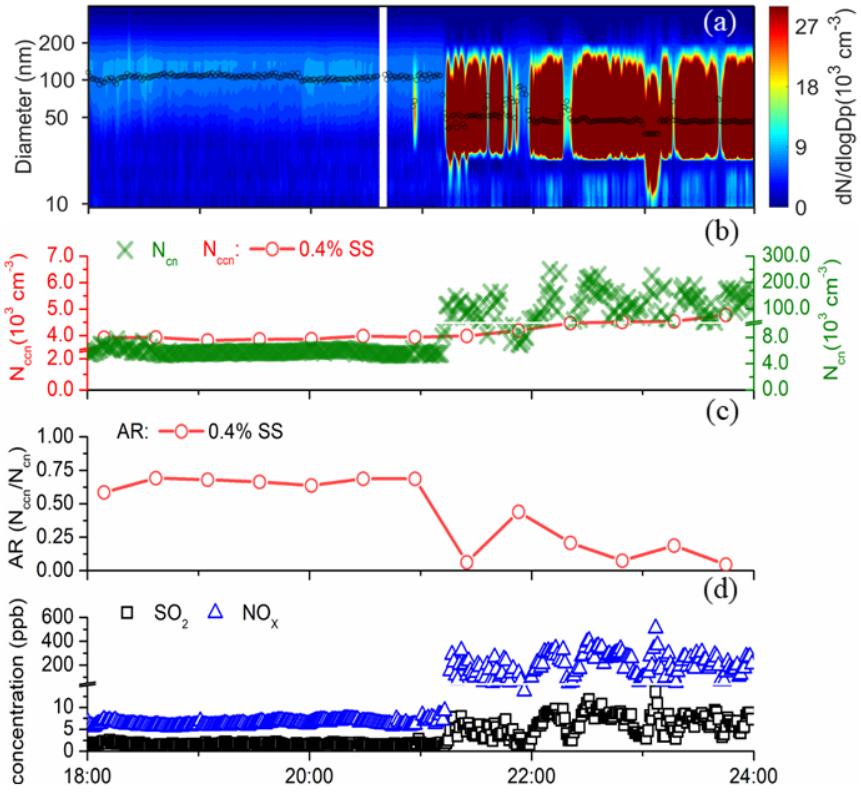

Fig 2 Contour plot of particle number size distribution with the median mobility mode diameter shown in black hollow circles (a), time series of minutely N_{cn} and half-hourly N_{ccn} at SS=0.4% (b), half-hourly AR values at SS=0.4% (c), SO_2 and NO_x at nighttime on DOY 115.

https://doi.org/10.5194/acp-2020-109
Preprint. Discussion started: 16 March 2020
© Author(s) 2020. CC BY 4.0 License.

Atmospheric Chemistry and Physics Discussions

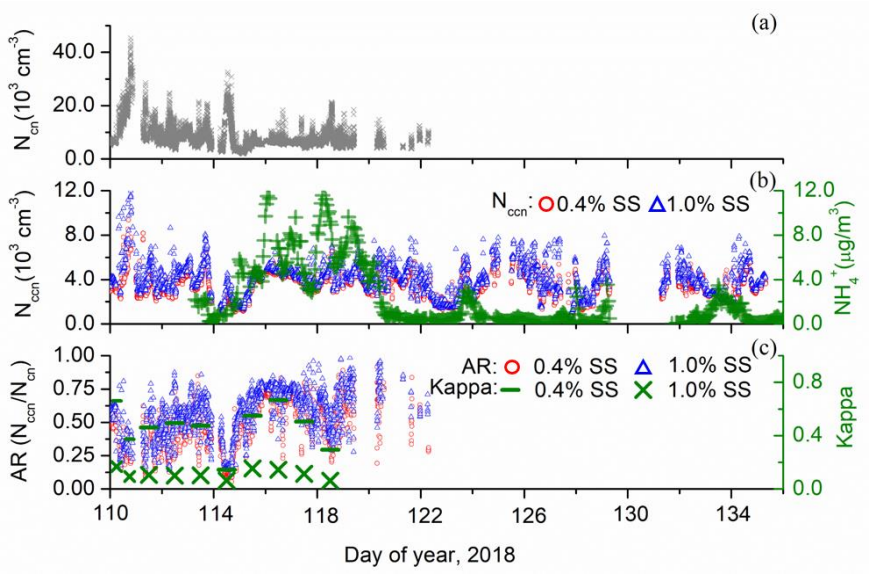

Fig 3 Time series of minutely N_{cn} from DOY 110 to 122 (a), minutely N_{ccn} at SS of 0.4% and 1.0% during DOY 110-135 and hourly NH_4^+ during DOY 113-135 (b), and minutely AR at SS of 0.4% and 1.0% during DOY 110-122 and daily *Kappa* values at SS of 0.4% and 1.0% from DOY 110 to 118 due to data availability (c). Please note that for Fig. 3c, most *Kappa* values were based on daily scale, except on DOY 110, during which two *Kappa* values were calculated from 00:00-06:00 and 08:00-21:00, respectively.

https://doi.org/10.5194/acp-2020-109
Preprint. Discussion started: 16 March 2020
© Author(s) 2020. CC BY 4.0 License.

Atmospheric Chemistry and Physics
Discussions

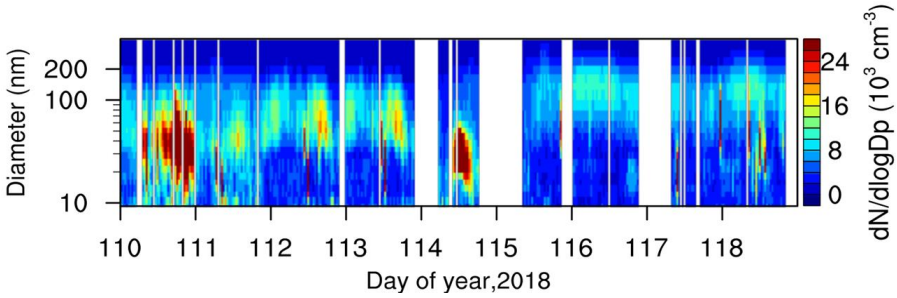

Fig 4 Contour plot of particle number size distribution on DOY 110-118 with self-ship emission signals removed.

https://doi.org/10.5194/acp-2020-109
Preprint. Discussion started: 16 March 2020
© Author(s) 2020. CC BY 4.0 License.

Atmospheric Chemistry and Physics
Discussions

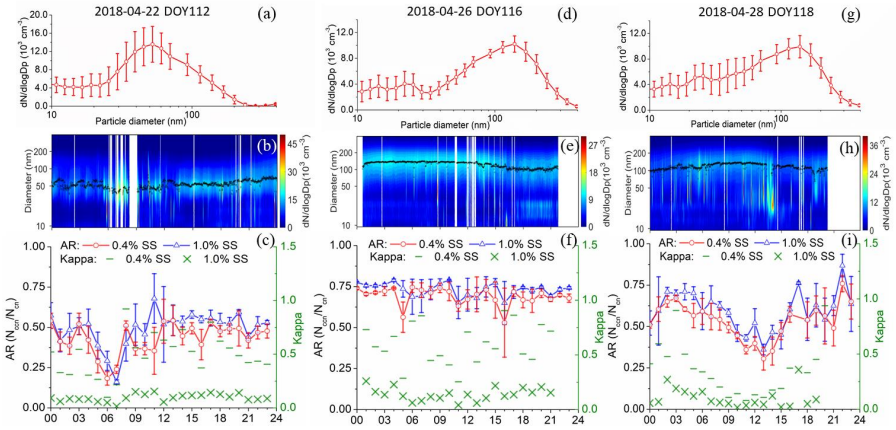

Fig 5 Daily average (top row) and contour plot (middle row) of particle number size distributions, and time series of hourly averaged AR at SS of 0.4% and 1.0% and *Kappa* value on DOY112, DOY116 and DOY118. The bars represent the standard deviation with mean indicated by the hollow circles.

https://doi.org/10.5194/acp-2020-109
Preprint. Discussion started: 16 March 2020
© Author(s) 2020. CC BY 4.0 License.

Atmospheric Chemistry and Physics Discussions

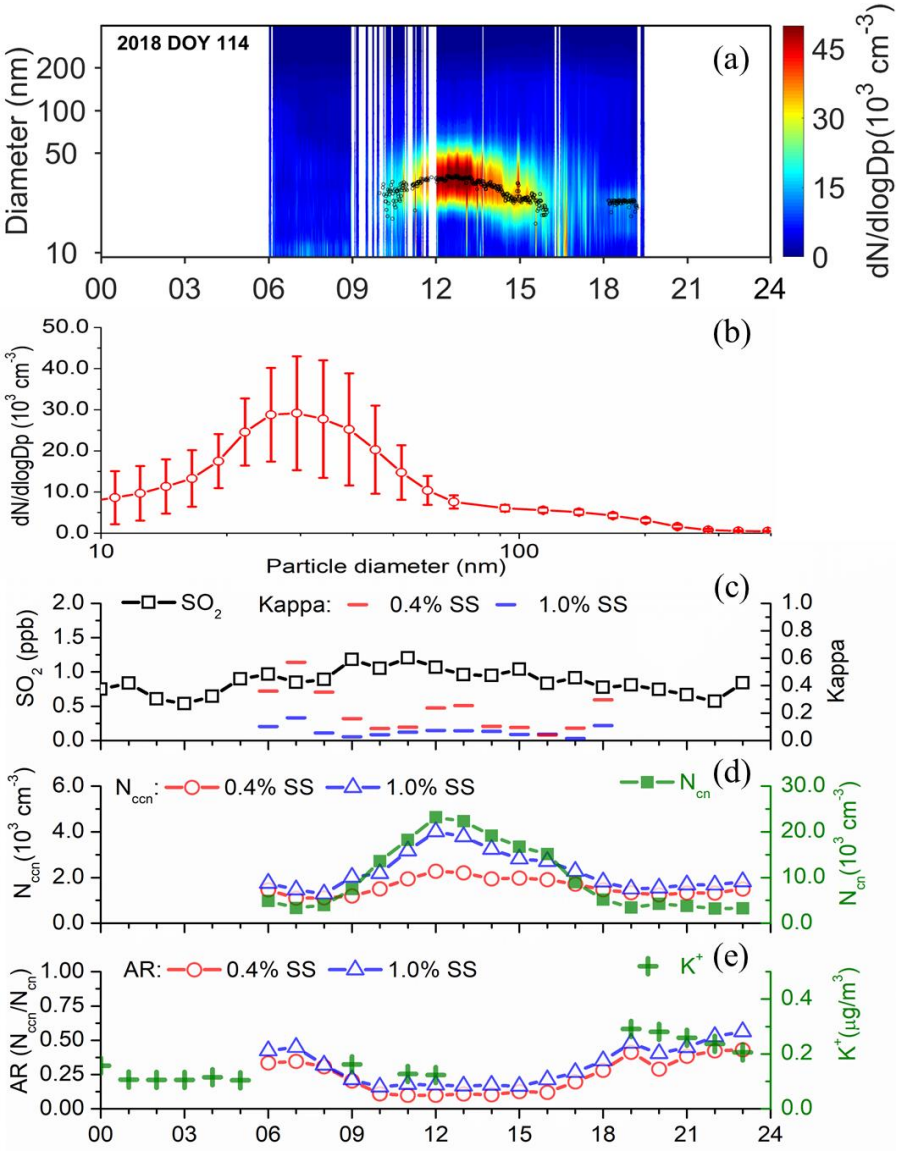

Fig 6 Contour plot of particle number size distributions for the day of DOY 114 2018 (a), the size distributions of particle number concentration during 10:00 -18:00 LT DOY 114 2018 (b), time series of hourly averaged SO_2 and *Kappa* values at SS of 0.4% and 1.0% (c), N_{ccn} at SS of 0.4% and 1.0% (d), and AR values at SS of 0.4% and 1.0% and K^+ (e) for the day of DOY 114 2018.

https://doi.org/10.5194/acp-2020-109
Preprint. Discussion started: 16 March 2020
© Author(s) 2020. CC BY 4.0 License.

Atmospheric Chemistry and Physics Discussions
Open Access

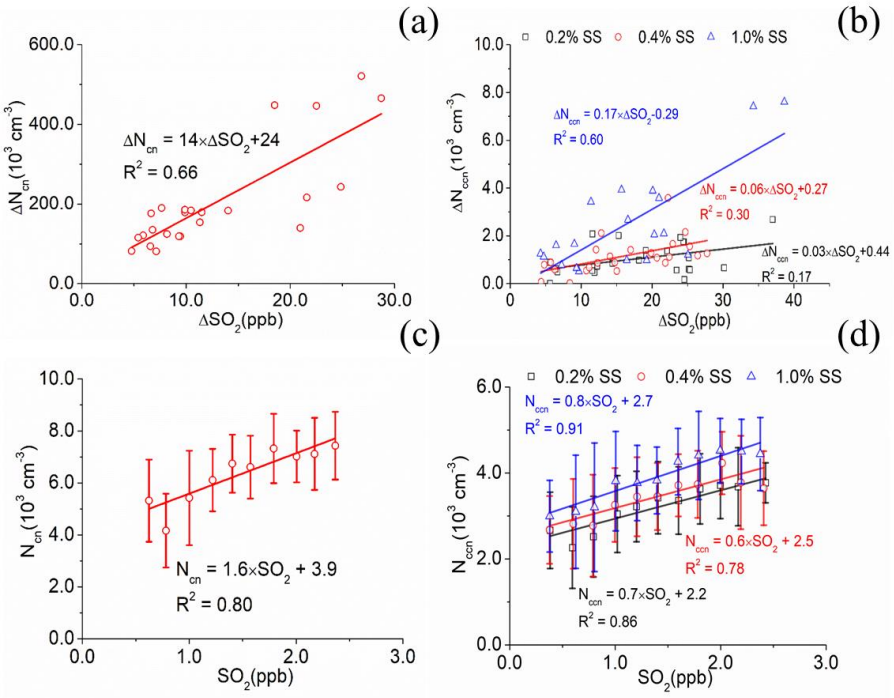

Fig 7 Correlations of hourly averaged N_{cn} and N_{ccn} with SO_2 at SS of 0.2%, 0.4% and 1.0%. For Fig. 7a,b, $\triangle N_{cn}$, $\triangle N_{ccn}$ and $\triangle SO_2$ reflects the impact from self-ship emission after the removal of ambient concentration. For Fig. 7c,d each bar indicates standard deviation with mean value marked as the hollow circles (or triangles, squares), and the interval of SO_2 is 0.2 ppb for each bar.

https://doi.org/10.5194/acp-2020-109
Preprint. Discussion started: 16 March 2020
© Author(s) 2020. CC BY 4.0 License.

Atmospheric Chemistry and Physics Discussions

Table 1. N_{cn} and N_{ccn}, AR and SO_2 mixing ratios on DOY 110-135, 2018 over China marginal seas. Please note that Ncn and AR are from 110-122, 2018.

Variables	Supersaturation (SS)	Ranges	Mean ± standard deviation
N_{cn} ($\times 10^3$ cm^{-3})		2.0-45	8.1±4.4
N_{ccn} ($\times 10^3$ cm^{-3})	SS=0.2%	0.4-8.8	3.2±1.1
	SS=0.4%	0.5-9.4	3.4±1.1
	SS=0.6%	0.5-8.6	3.6±1.2
	SS=0.8%	0.5-11	3.8±1.2
	SS=1.0%	0.6-12	3.9±1.4
AR	SS=0.2%	0.06-0.89	0.49±0.17
	SS=0.4%	0.06-0.92	0.51±0.17
	SS=0.6%	0.10-0.94	0.54±0.17
	SS=0.8%	0.08-0.95	0.56±0.17
	SS=1.0%	0.11-0.98	0.57±0.17
SO_2 (ppb)		0.25-9.7	1.7±1.1